BIOCHEMISTRY
including biophysical chemistry & molecular biology

Article

pubs.acs.org/biochemistry

Converting Transaldolase into Aldolase through Swapping of the Multifunctional Acid−Base Catalyst: Common and Divergent Catalytic Principles in F6P Aldolase and Transaldolase

Viktor Sautner, Mascha Miriam Friedrich, Anja Lehwess-Litzmann, and Kai Tittmann*

Göttingen Center for Molecular Biosciences, Department of Molecular Enzymology, Georg-August University Göttingen, Ernst-Caspari-Haus, Justus-von-Liebig-Weg 11, D-37077 Göttingen, Germany

ABSTRACT: Transaldolase (TAL) and fructose-6-phosphate aldolase (FSA) both belong to the class I aldolase family and share a high degree of structural similarity and sequence identity. The molecular basis of the different reaction specificities (transferase vs aldolase) has remained enigmatic. A notable difference between the active sites is the presence of either a TAL-specific Glu (Gln in FSA) or a FSA-specific Tyr (Phe in TAL). Both residues seem to have analoguous multifunctional catalytic roles but are positioned at different faces of the substrate locale. We have engineered a TAL double variant (Glu to Gln and Phe to Tyr) with an active site resembling that of FSA. This variant indeed exhibits aldolase activity as its main activity with a catalytic efficiency even larger than that of authentic FSA, while TAL activity is greatly impaired. Structural analysis of this variant in complex with the dihydroxyacetone Schiff base formed upon substrate cleavage identifies the introduced Tyr (genuine in FSA) to catalyze protonation of the central carbanion−enamine intermediate as a key determinant of the aldolase reaction. Our studies pinpoint that the Glu in TAL and the Tyr in FSA, although located at different positions at the active site, similarly act as bona fide acid−base catalysts in numerous catalytic steps, including substrate binding, dehydration of the carbinolamine, and substrate cleavage. We propose that the different spatial positions of the multifunctional Glu in TAL and of the corresponding multifunctional Tyr in FSA relative to the substrate locale are critically controlling reaction specificity through either unfavorable (TAL) or favorable (FSA) geometry of proton transfer onto the common carbanion−enamine intermediate. The presence of both potential acid−base residues, Glu and Tyr, in the active site of TAL has deleterious effects on substrate binding and cleavage, most likely resulting from a differently organized H-bonding network. Large-scale motions of the protein associated with opening and closing of the active site that seem to bear relevance for catalysis are observed as covalent intermediates are exclusively observed in the "closed" conformation of the active site. Pre-steady-state kinetics are used to monitor catalytic processes and structural transitions and to refine the kinetic framework of TAL catalysis.

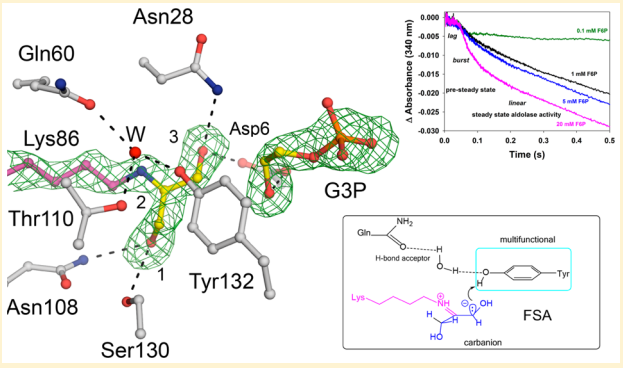

Transaldolase (TAL) and fructose-6-phosphate aldolase (FSA) both belong to the class I aldolase family, which operate via Schiff base chemistry using an active center lysine to reversibly cleave phosphoketose D-fructose-6-phosphate (F6P) in an aldol-type reaction.[1−3] Transaldolase shuttles a three-carbon dihydroxyacetone unit derived from F6P to aldose acceptor D-erythrose-4-phosphate (E4P), affording ketose D-sedoheptulose-7-phosphate (S7P) and aldose D-glyceraldehyde-3-phosphate (G3P) (eq 1).[1] FSA reversibly cleaves substrate F6P into G3P and dihydroxyacetone (DHA) (eq 2).[2] While F6P aldolase activity of FSA could be clearly demonstrated *in vitro*, its physiological function is still unclear.

$$\text{TAL: F6P + E4P} \Leftrightarrow \text{S7P + G3P} \quad (1)$$

$$\text{FSA: F6P} \Leftrightarrow \text{G3P + DHA} \quad (2)$$

The catalytic cycles of both enzymes are highly analogous and proceed through a series of identical covalent reaction intermediates, including the dipolar and neutral carbinolamine, the F6P Schiff base, and the carbanion−enamine intermediate with multiple critical proton transfers (Scheme 1).[3] Key to the different reaction specificities of the two enzymes is the stability of the carbanion−enamine intermediate formed upon cleavage of the common F6P Schiff base. While TAL retains the covalent C3−lysine carbanion−enamine conjugate bound in stable form for eventual transfer to aldose acceptor E4P (aldol addition), this intermediate undergoes facile hydrolysis in FSA, liberating DHA as a product. Aldolytic cleavage requires stereospecific protonation at C3 of the carbanion−enamine intermediate by a suitably placed acid−base catalyst followed by hydrolysis of the formed DHA Schiff base (Scheme 1).[3] The different reaction specificities of the two enzymes are very remarkable, because the overall structures as well as the active site architectures are

Received: March 16, 2015
Revised: June 11, 2015
Published: July 1, 2015

DOI: 10.1021/acs.biochem.5b00283
Biochemistry 2015, 54, 4475−4486

Scheme 1. Catalytic Cycles of TAL and FSA Showing Key Intermediates and Elementary Steps of Catalysis (see the text)[a]

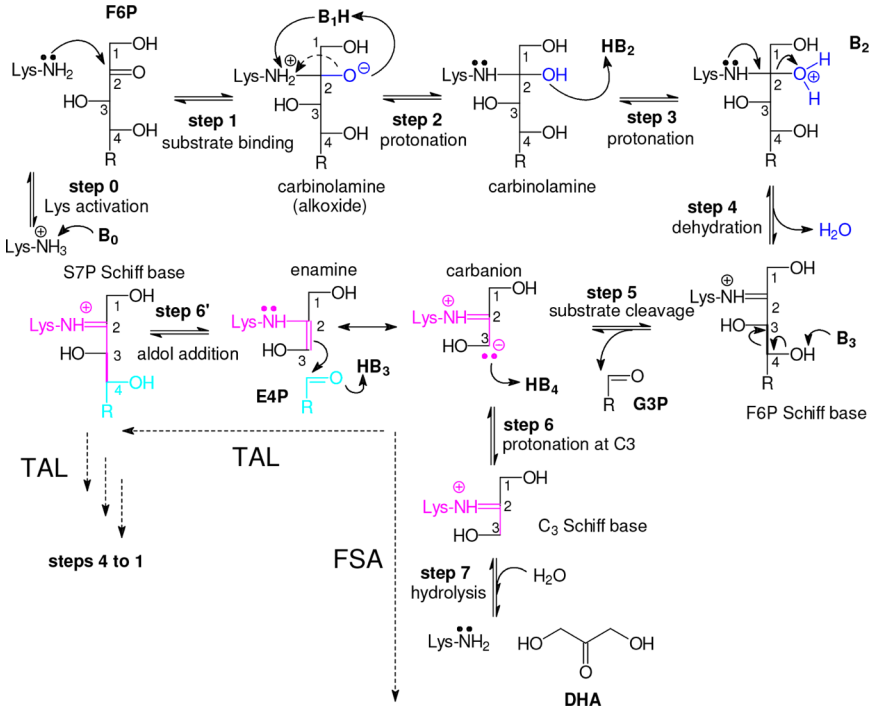

[a]Note that binding and processing of substrate F6P until the carbanion−enamine state (steps 1−5) are identical for both enzymes. While FSA catalyzes a protonation of C3 of the carbanion−enamine intermediate yielding the C3 (dihydroxyacetone) Schiff base (step 6), TAL prevents a protonation at C3 and rather promotes aldol condensation with an aldose acceptor (step 6′). Proton transfers and the action of associated acid−base catalysts are indicated.

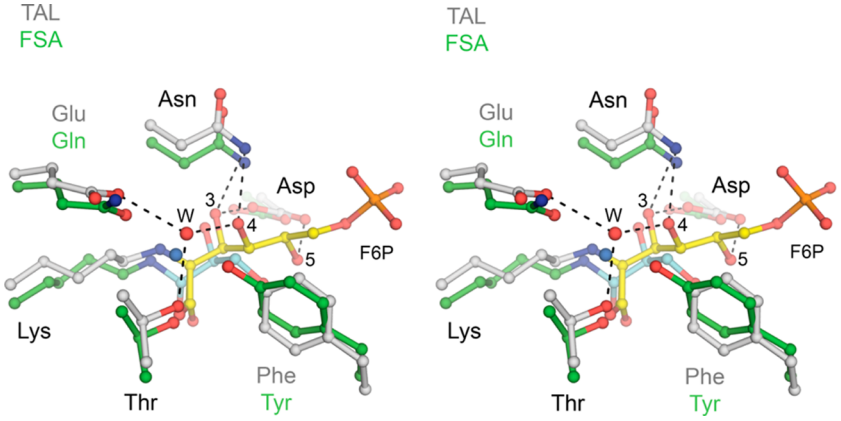

Figure 1. Active site structures of *Tac*TAL (PDB entry 3S1V) and *E. coli* FSA (PDB entry 1L6W) in stereoview. The active site of *Tac*TAL (colored gray) in complex with the F6P Schiff base (yellow) was superposed with that of *E. coli* FSA (green) in a covalent complex with glyceraldehyde (cyan) from the crystallization setup.[5,6] Selected active site residues and a catalytic water (water red for TAL and blue for FSA) are shown in ball-and-stick representation. Note that conserved residues are labeled in black, while nonconserved residues are colored either gray (*Tac*TAL) or green (*E. coli* FSA). Hydrogen-bonding interactions for the F6P Schiff base intermediate in *Tac*TAL are indicated by dashed lines.

highly equivalent (Figure 1). FSA from *Escherichia coli* has a similar overall structure [doughnut-shaped homodecamer of $(\beta/\alpha)_8$ barrels; *Z*-score of 30, root-mean-square deviation (rmsd) for Cα atoms of 1.5 Å for the monomer] and shows 31.1% sequence identity and 60.9% sequence similarity to TAL from *Thermoplasma acidophilum* (*Tac*TAL), of which several structures were recently determined at different stages of the catalytic cycle.[4,5] While most of the active site residues of *Tac*TAL with putative roles in substrate binding and catalysis are conserved in FSA (e.g., Asp6, Asn28, Lys86, Arg135, and Thr110), some active site residues are replaced in FSA by either hydrophobic (Ser130^{TAL} → Ala^{FSA}, Asn108^{TAL} → Leu^{FSA}, and Ser58^{TAL} → Phe^{FSA}) or homologous (Glu60^{TAL} → Gln^{FSA}, Phe132^{TAL} → Tyr^{FSA}, and Arg169^{TAL} → Lys^{FSA}) residues. The absence of Glu60 in the active site of *E. coli* FSA (Gln59) along with the presence of Tyr131 (Phe132 in *Tac*TAL) is of particular interest. Glu60 has been suggested to have a key catalytic role in multiple proton transfers in *Tac*TAL, including dehydration of the carbinolamine and substrate cleavage at the F6P Schiff base state by protonation of the 2-OH of the neutral carbinolamine and subsequent deprotonation of the 4-OH group of the F6P Schiff base (see Scheme 1).[5] This mechanism

DOI: 10.1021/acs.biochem.5b00283
Biochemistry 2015, 54, 4475−4486

seems to be conserved in the different TAL subfamilies.[6] The X-ray structures with bound substrate Schiff bases indicated that the proton transfers between Glu60 and the intermediates are shuttled through an adjacent catalytic water molecule (Figure 1). The absence of an equivalent Glu residue in the active site of FSA is therefore surprising, because the acid−base chemistry required for the aldol cleavage of substrate F6P is also part of the reaction pathway of this enzyme. With the exception of the conserved Asp6, only Tyr131 could potentially act as an acid−base catalyst in the active site of FSA. Because the structural studies of intermediates in transaldolase were suggesting a role of Asp6 in substrate binding and correct intermediate positioning with no direct role in proton transfers (it H-bonds to 3-OH and 5-OH of the substrate), we hypothesized that Tyr131 in FSA is a key acid−base catalyst of aldol cleavage akin to Glu60 in the reaction mechanism of TAL.[5] Tyr residues are already known to play crucial roles in proton-transfer reactions in other class I aldolases, most prominently in the case of mammalian fructose-1,6-bisphosphate (FBP) aldolase.[7,8] In, for example, rabbit muscle fructose-1,6-bisphosphate aldolase, the C-terminal tyrosine (Tyr363), which is located on a highly flexible segment, acts in concert with Lys146 and Glu187 as an acid−base catalyst during the hydrolytic cleavage of fructose 1,6-bisphosphate into dihydroxyacetone phosphate and G3P.[9] The deletion of this Tyr by treatment of the protein with carboxypeptidase resulted in a decrease in aldolase activity and an increase in transaldolase activity.[10] In archaeal aldolases, Tyr residues were shown to possess a multifunctional role akin to the conserved Glu in transaldolases and FBP aldolases from eukaryotes.[11,12] Recent studies demonstrated that an exchange of the aforementioned active site Phe in TAL of *E. coli* and of human origin (Phe132 in *Tac*TAL) by a Tyr greatly stimulated aldolase activity, while at the same time TAL activity was impaired.[13] Nonetheless, residual TAL activity in these variants was still 30−40-fold higher than aldolase activity. The exact role of this Tyr in substrate binding and catalysis of the Phe → Tyr TAL variants and in FSA remained, however, unclear. Modeling of the reaction intermediates trapped in *Tac*TAL into the active site of FSA suggested a potential role of the introduced Tyr as an acid−base catalyst in multiple proton transfers (dehydration, substrate cleavage, and protonation of the carbanion−enamine intermediate).[3] If this hypothesis were correct, the absence of an additional acid−base catalyst such as the TAL-specific Glu would likely be catalytically advantageous as two neighboring acid−base catalysts (a Glu and a Tyr) might obscure the required order and directionality of the numerous proton transfers due to a differently organized hydrogen-bonding network at the active site.

Here, we have examined the catalytic role of this Tyr residue in the FSA mechanism while using a transaldolase-derived "pseudo-FSA" enzyme, in which the TAL-specific key catalytic residues Glu60 and Phe132 in *Tac*TAL were changed to Gln60 and Tyr132, respectively, to restore an active site that closely resembles that of FSA. Our study underscores the role of this Tyr as a key acid−base catalyst in the FSA reaction using *Tac*TAL as a model by measurements of steady-state and transient kinetics, and high-resolution structural analysis of the central DHA Schiff base intermediate for the first time in this enzyme family. Remarkably, introduction of both mutations affords an enzyme variant (Glu60Gln/Phe132Tyr) with catalytic efficiency for F6P aldolase activity even higher than that for authentic FSA from *E. coli* and any TAL Phe-to-Tyr single variant tested so far. In a broader context, our studies delineate the governing principles of how the relative orientation of the multifunctional general acid−base catalyst to the reactive intermediate determines the different reaction specificities in aldolases and transaldolases.

MATERIALS AND METHODS

Mutagenesis, Expression, Purification, and Crystallization. Mutant strains producing *Tac*TAL variants Phe132-Tyr and Glu60Gln/Phe132Tyr were generated by introduction of appropriate mutations using the QuikChange site-directed mutagenesis protocol (Stratagene, La Jolla, CA). Expression and purification of *Tac*TAL wild type (wt) and both variants were conducted as described previously.[5,14] Double variant Glu60Gln/Phe132Tyr, which exhibits greatly increased aldolase activity, was crystallized according to the hanging-drop vapor-diffusion method using a reservoir solution of 200 mM ammonium acetate (pH 4.4), 10% (w/v) PEG 6000, and 25% (v/v) glycerol. To obtain crystal structures with reaction intermediates bound to the active site, *Tac*TAL double variant Glu60Gln/Phe132Tyr [16 mg/mL in 6 mM Tris-HCl and 14 mM glycylglycine (pH 7.5)] was supplemented with 34 mM F6P prior to crystallization; 3 μL of this solution was mixed with 3 μL of a reservoir solution at room temperature and equilibrated against 250 μL of a reservoir solution.

*Tac*TAL crystallizes in two different space groups ($P2_1$ and $C222_1$).[14] To grow sufficiently large single crystals of *Tac*TAL in the desired space group, $C222_1$, the crystallization solution was microseeded with previously obtained *Tac*TAL crystals of this space group and incubated at 30 °C for 10 min in a thermostated incubator. Transaldolase crystals were then further grown for 7−15 days at 20 °C.

X-ray Data Collection, Processing, and Model Building. Diffraction data of a single *Tac*TAL crystal (Glu60Gln/Phe132Tyr variant) were collected using synchrotron radiation at ESRF (beamline ID23-1, wavelength of 0.91 Å), Grenoble, France, at a cryogenic temperature of 100 K. Diffraction images were indexed, integrated, and scaled using the XDS package.[15]

Model building and refinement were performed using Coot and the Phenix.refine crystallographic package using the previously determined structure of *Tac*TAL wt as a starting model.[16−18] TLS grouping for each monomer was implemented as recently described.[5] The MolProbity server[19] was used to verify the geometry of the final model, of which 97.93% are in the favored region of the Ramachandran plot and 1.99% in the allowed region along with 0.09% outliers. The representation of structures was performed with PyMOL (Schrödinger, LLC).

The structural alignment of monomers of *Tac*TAL and FSA and the calculation of *Z*-score and the rmsd were performed using the DaliLite server[20] and T-Coffee server.[21]

Database Accession Number. The final refined model and the corresponding structure factor amplitudes have been deposited in the Research Collaboratory for Structural Biology (http://www.rcsb.org) as entry 4XZ9.

Steady-State Activity Assay. The steady-state kinetics for aldolase activity of *Tac*TAL wt and variants (conversion of donor F6P into G3P and DHA) were measured in a coupled spectrophotometric assay using the auxiliary enzymes triosephosphate isomerase (TIM) and *sn*-glycerol-3-phosphate:-NAD^+ 2-oxidoreductase (G3PDH) to detect formation of G3P formed by aldolytic cleavage of F6P.[22] The concomitant oxidation of NADH was monitored spectrophotometrically in a

DOI: 10.1021/acs.biochem.5b00283
Biochemistry 2015, 54, 4475−4486

UV−vis spectrometer (V-650, Jasco GmbH, Gros-Umstadt, Germany) at 340 nm and 30 °C. The reaction mixture contained 20 mM glycylglycine (pH 7.5), 3 units/mL TIM/G3PDH [8 mM $(NH_4)_2SO_4$], 0.22 mM NADH, and varying concentrations of F6P (0.1−100 mM). The enzyme concentrations were 1 mg/mL (*Tac*TAL wt), 0.17 mg/mL (*Tac*TAL Phe132Tyr), and 0.035 mg/mL (*Tac*TAL Glu60Gln/Phe132Tyr).

Transaldolase activity was analyzed under the same conditions except that acceptor E4P was added to the assay at concentrations of ≤2 mM.

To determine the macroscopic kinetic constants (k_{cat} and K_M), the initial rates were plotted against substrate concentration and analyzed using the Michaelis−Menten equation.

Pre-Steady-State Kinetics. The presteady state of the donor half-reaction (cleavage of donor F6P) was analyzed by stopped-flow kinetics using a coupled spectrophotometric assay as described above. The enzyme solution [0.44 mg/mL *Tac*TAL, 200 units/mL TIM/G3PDH, and 0.44 mM NADH in 20 mM glycylglycine (pH 7.5)] and the substrate solution [0.1−100 mM F6P in 20 mM glycylglycine (pH 7.5)] were rapidly mixed using a stopped-flow spectrometer (SX20, Applied Photophysics) in a 1 + 1 mixing ratio at 30 °C. Progress curves were fitted with appropriate equations consisting of either one or two single-exponential terms (pre-steady-state phase) and a linear term (steady-state consumption of F6P) (*vide infra*).

The estimated rate constants k_{obs} of the pre-steady-state phase were plotted versus the applied F6P concentration, and data were fitted to either a hyperbolic equation (eq 3) for F6P concentrations of ≤12 mM or a hyperbolic equation taking into account substrate access inhibition (eq 4).

$$k_{obs} = \frac{k_{obs}^{max}[F6P]}{K_S^{app} + [F6P]} \quad (3)$$

$$k_{obs} = \frac{k_{obs}^{max}}{1 + \frac{K_S^{app}}{[F6P]} + \frac{[F6P]}{K_I}} \quad (4)$$

where k_{obs}^{max} denotes the rate constant at infinitely high F6P concentrations, K_S^{app} the equilibrium constant of the fast substrate binding (pre)equilibrium, and K_I the inhibition equilibrium constant of a putative substrate access inhibition.

RESULTS AND DISCUSSION

Steady-State Kinetic Analysis of Aldolase and Transaldolase Activity. *Tac*TAL wt and *Tac*TAL variants Phe132Tyr and Glu60Gln/Phe132Tyr could be recombinantly expressed in *E. coli* and purified to homogeneity. The expression yields of the two variants were not as high as in the case of the wt enzyme (~2 mg of enzyme/g of cell pellet) and amounted to 0.8 mg of enzyme/g of cell pellet for Phe132Tyr or even 0.3 mg of enzyme/g of cell pellet in the case of Glu60Gln/Phe132Tyr.

We first assessed the steady-state kinetic properties of all three proteins for F6P aldolase activity (F6P as the sole substrate) and TAL activity (F6P and E4P as substrates) using a spectrophotometric assay that detects liberated product G3P. *Tac*TAL wt exhibits a very small yet detectable F6P aldolase activity that corresponds to a k_{cat} of ~2.2×10^{-3} s^{-1} on a per active site basis (Table 1). However, because very high concentrations of the enzyme were required in the assay, true steady-state (multiple-turnover) conditions cannot be established at low F6P concentrations, precluding a reliable estimation of the K_M^{F6P} value. Notably, the aldolase activity of *Tac*TAL wt is 3−4 orders of magnitude smaller than its genuine TAL activity (k_{cat} ~ 14 s^{-1}). Single variant Phe132Tyr exhibits a 10^2-fold stimulated F6P aldolase activity (k_{cat} = 0.24 ± 0.01) and a K_M value for F6P (12.3 ± 1.5 mM) that is comparable to that of FSA (Table 1 and Figure 2). The catalytic efficiency k_{cat}/K_M of *Tac*TAL Phe132Tyr is approximately 5% of that of FSA. The TAL activity of this variant is greatly impaired, and addition of acceptor E4P (tested up to 2 mM at different F6P concentrations) to the F6P-containing assay did not lead to a measurable change in the reaction rate, suggesting that the TAL activity is smaller than (or equal to) the FSA activity. This translates into a reduction of TAL activity by a factor of at least ~60 in this variant. Introduction of the second mutation into the Glu60Gln/Phe132Tyr double variant

Table 1. Steady-State Kinetic Parameters of Aldolase (cleavage of F6P into DHA and G3P) and TAL (F6P + E4P → S7P + G3P) Activity of *Tac*TAL wt and Variants in Comparison to Those of FSA and Previously Studied Variants from *E. coli* and Human TAL

protein	k_{cat} (s^{-1})	K_M^{F6P} (mM)	k_{cat}/K_M (M^{-1} s^{-1})
	FSA Activity		
*Tac*TAL wt	(2.25 ± 0.01) × 10^{-3}	nd	nd
*Tac*TAL Phe132Tyr	0.24 ± 0.01	12.3 ± 1.5	19.5
*Tac*TAL Glu60Gln/Phe132Tyr	0.62 ± 0.01	1.5 ± 0.1	413
*Ec*FSA[a]	1.30 ± 0.30	12.0 ± 3.0	108
*Ec*TAL Phe178Tyr[a]	0.22 ± 0.03	1.5 ± 0.2	147
*Hs*TAL Phe189Tyr[a]	0.21 ± 0.02	0.76 ± 0.11	276
	TAL Activity[b]		
*Tac*TAL wt	13.86 ± 0.65	2.30 ± 0.36	6026.1
*Tac*TAL Phe132Tyr	≤0.24	nd	nd
*Tac*TAL Glu60Gln/Phe132Tyr	<0.62	nd	nd
*Ec*TAL wt[a]	53 ± 6	3.0 ± 0.2	17666
*Hs*TAL wt[a]	18	2.3	7826
*Ec*TAL Phe178Tyr[a]	8.8 ± 0.5	22 ± 5	400
*Hs*TAL Phe189Tyr[a]	7.4 ± 1.1	27 ± 4	274

[a]Taken from ref 13. [b]In the presence of 2 mM E4P.

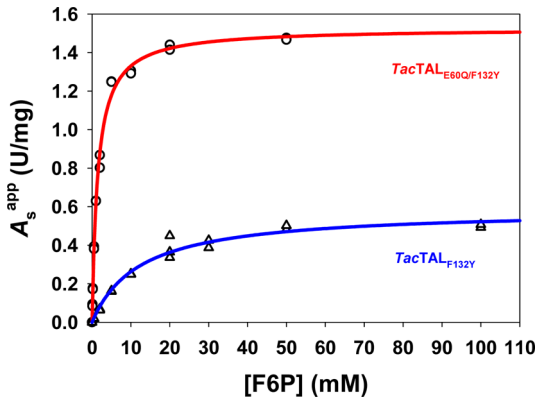

Figure 2. Steady-state kinetic analysis of F6P aldolase activity of *Tac*TAL variants Phe132Tyr (△) and Glu60Gln/Phe132Tyr (○) showing the substrate dependence of specific activity A_S and corresponding fits according to the Michaelis−Menten equation (Phe132Tyr, blue; Glu60Gln/Phe132Tyr, red).

DOI: 10.1021/acs.biochem.5b00283
Biochemistry 2015, 54, 4475−4486

Scheme 2. Minimal Kinetic Scheme of TAL/FSA-Catalyzed Cleavage of F6P into G3P and DHA Indicating the Two Half-Reactions and Conformational Dynamics (see the text)[a]

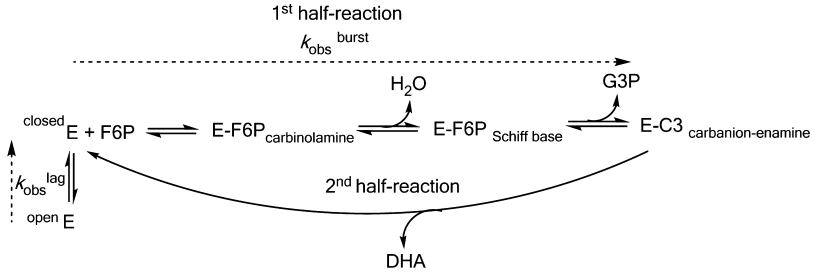

[a]Note that the first half-reaction is on pathway in TAL and FSA, whereas the second half-reaction is off pathway in TAL but on pathway in FSA. In case of *Tac*TAL double variant Glu60Gln/Phe132Tyr, an additional substrate-independent lag phase that likely reflects the conformational dynamics of the protein that samples between an "open" and "closed" state was observed (see the text). This lag phase was not observed for *Tac*TAL wt and for single variant Phe132Tyr using stopped-flow kinetics.

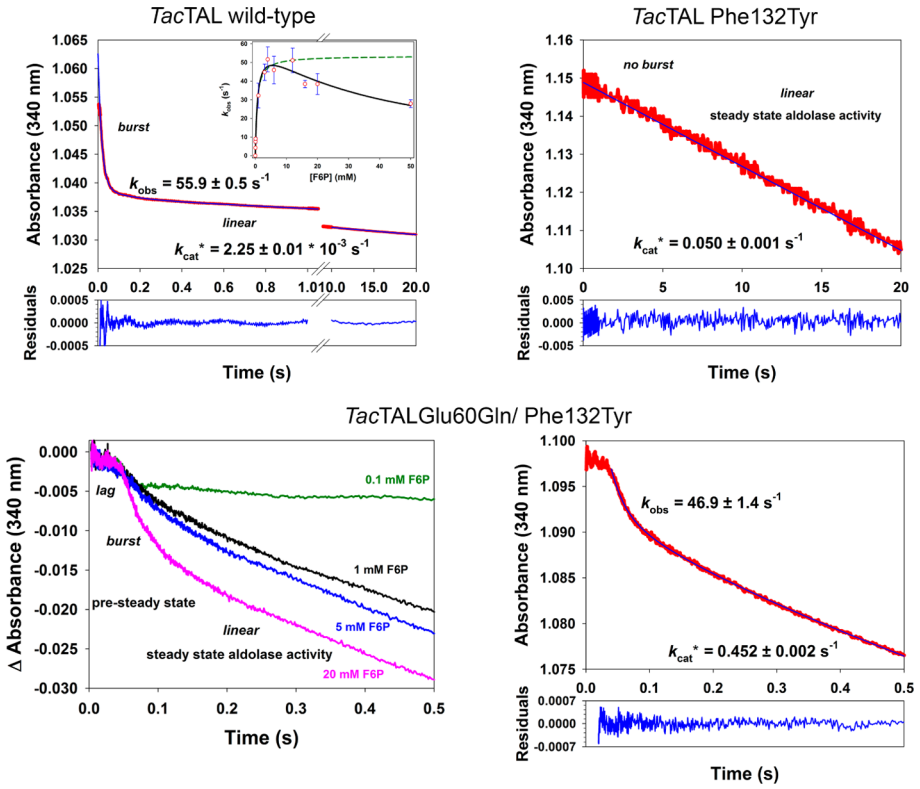

Figure 3. Pre-steady-state kinetic analysis of *Tac*TAL-catalyzed cleavage of F6P into G3P and DHA (for conditions, see Materials and Methods). The top left panel is a representative progress curve recorded at 340 nm after mixing *Tac*TAL wt with 10 mM F6P (final concentration). The data were fit with an equation comprising a single exponential (burst phase) and a linear term (steady-state depletion of substrate). The inset shows the dependence of the observed rate constant of the burst phase (k_{obs}) on the applied F6P concentration using a hyperbolic function taking into account substrate access inhibition (black solid line). Alternatively, data at F6P concentrations of ≤12 mM were fitted to a simple hyperbolic function (green dashed line). The top right panel is a representative progress curve recorded at 340 nm after mixing *Tac*TAL variant Phe132Tyr with 10 mM F6P (final concentration). Note the absence of a burst phase. Data were fitted with a linear regression. The bottom left panel shows representative progress curves at 340 nm obtained after mixing *Tac*TAL double variant Glu60Gln/Phe132Tyr with either 0.1, 1, 5, or 20 mM F6P (final concentration). Note the appearance of a lag phase (duration not dependent on applied F6P concentration) and of a subsequent burst phase prior to the linear signal decrease at the steady state (see Scheme 2). The bottom right panel shows the progress curves fit with an equation comprising a single exponential (burst phase) and a linear (steady-state depletion of substrate) term.

increases F6P aldolase activity by an additional factor of 3 (k_{cat} = 0.62 ± 0.01 s^{-1}) and at the same time decreases the apparent Michaelis constant of F6P (K_M = 1.5 ± 0.1 mM) compared to that of the Phe132Tyr single variant (Table 1 and Figure 2). Addition of acceptor E4P (tested up to 2 mM) to the assay containing F6P resulted in a decrease in the reaction rate by up to 10%, showcasing the fact that (i) TAL activity is smaller than FSA activity and (ii) bound E4P slightly impairs protonation of the carbanion−enamine intermediate and/or hydrolysis of the C3 Schiff base (see Scheme 1). Notably, the catalytic efficiency of F6P aldolytic cleavage for *Tac*TAL double variant Glu60Gln/Phe132Tyr (413 M^{-1} s^{-1}) is the highest ever reported; it is higher than these of authentic FSA and of Phe → Tyr single variants from *E. coli* and human TAL (Table 1).[13]

DOI: 10.1021/acs.biochem.5b00283
Biochemistry 2015, 54, 4475−4486

Although these previously studied variants exhibited markedly elevated FSA activity, their residual TAL activity was still 30−40-fold higher than their FSA activity. In the case of *Tac*TAL double variant Glu60Gln/Phe132Tyr, the FSA activity is clearly higher than the residual TAL activity as indicated by the observed inhibitory effect of E4P on F6P consumption.

Pre-Steady-State Kinetic Analysis of F6P Conversion. To gather more insights into the kinetics of *Tac*TAL-catalyzed F6P cleavage, we conducted stopped-flow experiments in which *Tac*TAL was mixed with substrate F6P. In a minimal reaction scheme (Scheme 2), aldolytic cleavage of F6P into products G3P and DHA can be subdivided into two half-reactions: (i) F6P binding and cleavage (all steps until liberation of G3P) and (ii) protonation and hydrolysis of the C3 carbanion−enamine intermediate with concomitant release of DHA. Because midway-formed product G3P is detected in the spectrophotometric assay, the potential occurrence or absence of a pre-steady-state phase is diagnostic for which of the two half-reactions is rate-determining for overall catalysis akin to the classic kinetic analysis of protease-catalyzed turnover of *p*-nitrophenyl ester substrates.[23,24]

When *Tac*TAL wt was mixed with substrate F6P in the stopped-flow instrument, an initial pre-steady-state burst phase was observed in the first 100 ms followed by a linear decrease in absorbance in the steady state (Figure 3). This observation indicates that the second half-reaction (protonation of the carbanion−enamine intermediate, hydrolysis of DHA Schiff base, and DHA release) is rate-determining for the overall reaction, whereas the first half-reaction that is binding and cleavage of F6P proceeds considerably faster. The fitted first-order rate constants (k_{obs}) of the burst phase display a hyperbolic dependence on the substrate concentration up to 10 mM with a K_S^{app} of 0.49 ± 0.06 mM; at higher F6P concentrations, however, rate constants are getting smaller. The reason for the slowed substrate binding and/or cleavage at high F6P concentrations is unclear; this observation could reflect substrate access inhibition or, alternatively, a negative cooperativity between the different monomers (*Tac*TAL forms homopentamers assembling into decamers) as suggested by previous structural studies.[5] In support of this mechanistic proposition invoking an intermonomer negative cooperativity is the finding that the maximal amplitude of the burst phase corresponds to turnover of only 60% of the active sites, indicating that at a maximum only three of five monomers of the pentamer are acting on F6P. Alternatively, a switch between an induced fit and a conformational selection mechanism at higher F6P concentrations might account for the observed dependence of k_{obs} on the F6P concentration.[25] The maximal rate constant k_{obs} of the burst phase amounts to ∼50−55 s^{-1} (at c_{F6P} values of 5−15 mM), which is greater than the turnover number for the overall TAL reaction (k_{cat} ∼ 14 s^{-1}). This pinpoints that all reaction steps until formation of the carbanion−enamine intermediate are not rate-determining for the TAL reaction. This in turn suggests that aldol addition of the carbanion−enamine intermediate with acceptor E4P and subsequent liberation of product S7P must be (at least partially) rate-determining for the overall TAL reaction. As expected, off-pathway protonation of the carbanion−enamine intermediate and subsequent DHA liberation proceed extremely slowly in *Tac*TAL wt and are rate-determining for conversion of F6P into G3P and DHA (k' = 2.25 × 10^{-3} s^{-1}).

In *Tac*TAL single variant Phe132Tyr, no burst phase can be observed in the stopped-flow kinetic analysis of F6P conversion (Figure 3). As it could be established that a burst is not occurring in the dead time of the stopped-flow experiment (t ∼ 1.5 ms), this observation indicates that the single-site Phe132 → Tyr substitution in *Tac*TAL greatly impairs one or more step(s) of the first half-reaction comprising all steps until formation of the carbanion−enamine intermediate and concomitant G3P release. Because of this kinetic behavior, the first half-reaction that is binding and cleavage of F6P has become rate-determining in the variant (k_{obs} ≤ 0.24 s^{-1}) and thus proceeds at least 200-fold slower than in the wild-type enzyme (k_{obs}^{max} = 55 s^{-1}). This drastic effect implies that the Phe → Tyr single-site mutation has a large impact on the active site structure and/or reactivity.

*Tac*TAL double variant Glu60Gln/Phe132Tyr exhibits a pre-steady-state phase that is similar to that of *Tac*TAL wt as a pre-steady-state burst phase preceding a linear decrease in the steady state can be observed (Figure 3). However, in addition, a lag phase can be monitored in the very first 50 ms of the reaction. Notably, the duration of this lag phase is not dependent on the applied substrate concentration, suggesting that this kinetic phase reflects an intrinsic process of the enzyme. There is precedent in the literature for substrate-independent lag phases as, for example, in the case of glucanase.[26] Because the previous structural analysis of *Tac*TAL showed the enzyme to adopt an open (presumably inactive) and closed (presumably active) conformation with an equilibrium position close to unity in the resting state,[5] one might speculate that the observed lag phase corresponds to the equilibrium shift between the two states upon substrate binding according to a conformational selection mechanism (Scheme 2).[27,28] The fitted first-order rate constants of the burst phase show a similar dependence on the F6P concentration as described above for the wild-type enzyme with a k_{obs}^{max} of ∼50 s^{-1} [e.g., at 10 mM F6P, k_{obs} = 46.9 ± 1.4 s^{-1} (see Figure 3)]. The preceding lag phase can be reasonably fitted at F6P concentrations of >5 mM with a single-exponential function and amounts to 50−70 s^{-1} for the individual progress curves [e.g., k_{obs}^{lag} = 67.2 ± 3.7 s^{-1} at 10 mM F6P (see Figure 3)]. Admittedly, at lower F6P concentrations, the k_{obs} of the lag phase cannot be reliably estimated because of the very small amplitude of this phase, such that a precise value cannot be determined with this type of experiment. In summary, introduction of the second mutation (Glu60 → Gln) in the *Tac*TAL double variant Glu60Gln/Phe132Tyr restored the active site in a way in which F6P binding and cleavage are as efficient as in the wild-type enzyme, whereas the single variant Phe132Tyr with both potential acid−base catalysts at the active site (Glu60 and Tyr132) is greatly impaired in that regard. The second half-reaction of aldolytic F6P cleavage (see Scheme 2) in *Tac*TAL Glu60Gln/Phe132Tyr is rate-determining for the overall reaction [k_{cat} = 0.62 s^{-1} (see Table 1)], pinpointing that protonation of the carbanion−enamine intermediate, hydrolysis of the C3 (DHA) Schiff base, and/or product release is the slowest step of catalysis. Interestingly, we can observe kinetic processes (initial lag phase) with this variant that are independent of the applied substrate concentration, tempting us to identify these processes as intrinsic protein dynamics and/or conformational changes of reversible opening ⇔ closing and substrate binding according to a conformational selection mechanism as previously suggested.[5] We did not observe this lag phase in the case of the wt TAL enzyme, suggesting that these processes proceed considerably faster and cannot be resolved by stopped-flow experiments (dead time of 1.5 ms).

DOI: 10.1021/acs.biochem.5b00283
Biochemistry 2015, 54, 4475−4486

Although F6P is efficiently bound and cleaved in the double variant [k_{obs} ~50 s^{-1} (see Figure 3)], TAL activity is greatly impaired as evidenced by the inhibitory effect of E4P on F6P consumption [k_{cat} < 0.62 s^{-1} (data not shown)]. This suggests that this variant binds E4P in a nonproductive conformation or, alternatively, that the carbanion−enamine intermediate has undergone rapid protonation at C3 (the conjugate acid would be unreactive toward aldol acceptors).

Structural Analysis of *Tac*TAL Glu60Gln/Phe132Tyr in Complex with the Covalent Dihydroxyacetone Schiff Base Intermediate. The crystal structure of *Tac*TAL double variant Glu60Gln/Phe132Tyr (cocrystallized with substrate F6P) was determined using the structure of *Tac*TAL wt (PDB entry 3S0C) as the initial model for rigid-body refinement and was refined to R_{work} and R_{free} values of 16.22 and 19.38%, respectively, against data to 1.80 Å resolution (Table 2). While

Table 2. Data Collection and Refinement Statistics for *Tac*TAL E60Q/F132Y with a DHA Schiff Base

Data Collection[a]	
space group	$C222_1$
cell dimensions	
a, *b*, *c* (Å)	148.9, 172.1, 100.2
α, *β*, *γ* (deg)	90.0, 90.0, 90.0
resolution (Å)	49.08−1.80 (1.90−1.80)
R_{sym}, R_{merge} (%)	4.1, 41.0
$I/\sigma I$	23.26 (3.96)
completeness (%)	99.9 (99.9)
redundancy	5.6 (5.7)
Refinement	
resolution (Å)	49.08−1.80
no. of reflections	118566
R_{work}, R_{free} (%)	16.22, 19.38
no. of atoms	
protein (chain A/B/C/D/E)	1880/1704/1780/1924/1749
DHA/G3P (B/C)	13/13
other ligands	46
waters	750
B factor (Å^2)	
protein (A/B/C/D/E)	39.76/36.75/33.77/34.29/39.14
DHA/G3P (B/C)	43.00/38.79
other ligands	39.38
waters	43.48
rmsd	
bond lengths (Å)	0.014
bond angles (deg)	1.363
B factor from the Wilson plot (Å^2)	26.61

[a]Data for the highest-resolution shell are shown in parentheses.

subunits B and C of the pentamer in the asymmetric unit exhibit very well-defined electron density for all residues and adopt the "closed" conformation, subunits A, D, and E are structurally flexible, and their N-terminal parts (residues 1−55) could be modeled for some parts as a mixture of the "open" and "closed" states (*vide infra*). Inspection of the electron density maps in the active sites of the well-defined "closed" subunits B and C clearly indicates that the catalytic Lys86 is in covalent linkage with a three-carbon moiety, very likely derived from cleavage of the F6P Schiff base (Figure 4a). In addition to the covalent reaction intermediate, density is detectable at the active site that suggests the presence of product G3P formed upon cleavage of the F6P Schiff base. The electron density around G3P is not as well-defined as for the covalent conjugate and interacting active side residues; while the phosphate portion and the neighboring C-OH group of G3P can be modeled into the density, there is no traceable defined electron density for the aldo group, suggesting some structural flexibility of bound G3P. After final refinement, weak positive difference electron density could be detected close to the C-OH group of G3P that might correspond to the C1 aldo portion, but it could also result from a resting-state placeholder water (data not shown). It is interesting to note that in the *Tac*TAL Glu60Gln/Phe132Tyr crystal, product G3P and the covalent C3−lysyl conjugate are not recombining to give the F6P Schiff base as previously observed for *Tac*TAL wt, where cocrystallization with F6P under identical conditions led to predominant accumulation of the F6P Schiff base *in crystallo*. This observation renders accumulation of the C3 carbanion−enamine intermediate in the double variant unlikely (it would likely collapse with adjacent aldose acceptors) but rather suggests that the conjugate acid of the carbanion-enamine intermediate, the C3-protonated dihydroxyacetone (DHA) Schiff base, has accumulated in the crystal (see Scheme 1).

*Tac*TAL Glu60Gln/Phe132Tyr (aldolase activity):

substrate cleavage protonation at C3

$$E_{F6P\ Schiff\ base} \rightleftharpoons E_{carbanion\text{-}enamine} + G3P \rightleftharpoons E_{DHA\ Schiff\ base} + G3P$$

accumulated

*Tac*TAL wt (genuine transaldolase activity):

substrate cleavage protonation at C3

$$E_{F6P\ Schiff\ base} \rightleftharpoons E_{carbanion\text{-}enamine} + G3P \rightarrow\!\!\!\!\times\ E_{DHA\ Schiff\ base} + G3P$$

accumulated

In agreement with this tentative assignment, the geometry of the three-carbon moiety is not compatible with an enamine as the 3-OH group of the intermediate is not in plane (~50° out of plane) with the C2−Nε bond as would be expected for an enamine (see Scheme 1). This suggests that C3 of the intermediate is sp^3-hybridized. At this resolution, it seems impossible to differentiate between a carbanion and the protonated form (both would have sp^3-hybridized C3); however, we believe that a carbanion would immediately recombine with an adjacent acceptor, and its accumulation is thus an unlikely scenario (see above). The DHA Schiff base is firmly held in place through numerous H-bonding interactions with active side residues. While its 1-OH group H-bonds to the side chains of Asn108 and Ser130, the 3-OH group interacts with Asp6 and Asn28 at the opposite structural face of the active site (Figure 4a). The catalytic water is bound atop C2 of the DHA Schiff base intermediate in striking distance (2.96 Å) for eventual attack in the course of hydrolytic cleavage and is coordinated by Gln60, Thr110, and Tyr132 (Figure 4b). Both the calculated electron density maps and the Molprobity-based analysis of local interactions suggest that the carboxamide O of Gln60 is H-bonding to the catalytic water. Tyr132 is very likely acting as the acid−base catalyst trapping the incipient carbanion at C3 formed upon cleavage of the F6P Schiff base by protonation. Although the interatomic distance between the Tyr-OH group and C3 of the intermediate is slightly too long

DOI: 10.1021/acs.biochem.5b00283
Biochemistry 2015, 54, 4475−4486

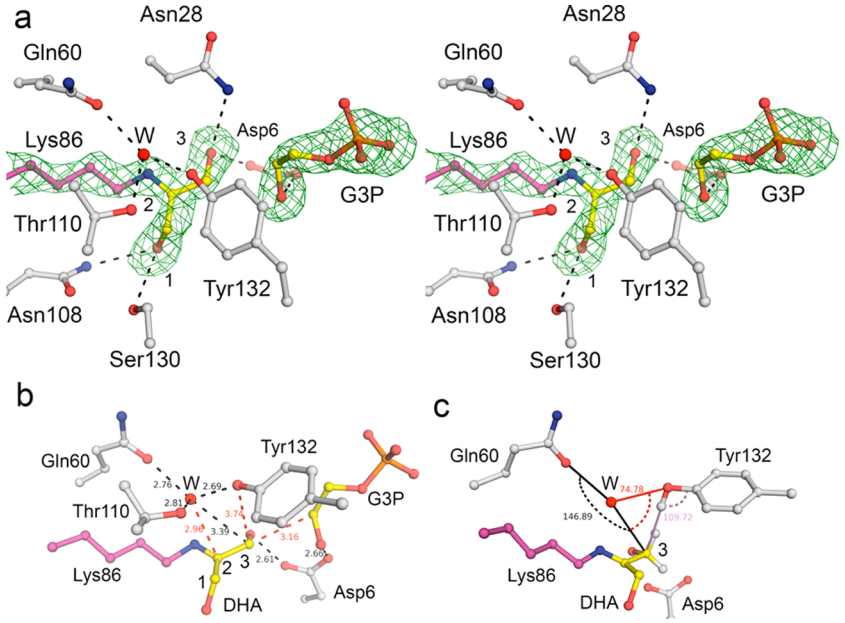

Figure 4. Structure of the dihydroxyacetone (DHA) Schiff base intermediate and of product G3P in *Tac*TAL variant Glu60Gln/Phe132Tyr. (a) Structure of the DHA Schiff base and of G3P in stereoview and ball-and-stick representation. The $mF_o - DF_c$ omit map around the covalent lysyl conjugate and G3P is colored green at a contour level of 2.5σ (Lys86, the DHA moiety, and G3P were excluded from the model for map calculation). Hydrogen bonds of <3.3 Å are indicated by dashed lines. The sugar moieties are colored yellow, and Lys86 is colored magenta. The catalytic water (denoted as "W") is shown as a red sphere. (b) Structure of the DHA Schiff base and G3P in *Tac*TAL highlighting the lengths of H-bonding interactions (black) and reacting moieties (red). (c) Structure of the DHA Schiff base in *Tac*TAL showing the angles for either a direct proton transfer between Tyr132 and DHA-C3 ($C4_{Tyr}–O_{Tyr}–C3_{DHA}$ angle, magenta) or a synchronized proton transfer from Tyr132 via the catalytic water ($O_{Tyr}–O_W–C3_{DHA}$ angle, red). The two hydrogen atoms at C3 of the DHA Schiff base and that of the Tyr-OH group were added in their corresponding riding positions. Note that protonation at C3 of the carbanion–enamine intermediate occurs stereospecifically (upper hydrogen at C3), thus favoring a direct proton transfer between Tyr132 and C3 caused by optimal geometry. A potential proton transfer from Glu60 (mutated to Gln60 in the variant) to DHA-C3 in *Tac*TAL wt is geometrically not favorable (see the text).

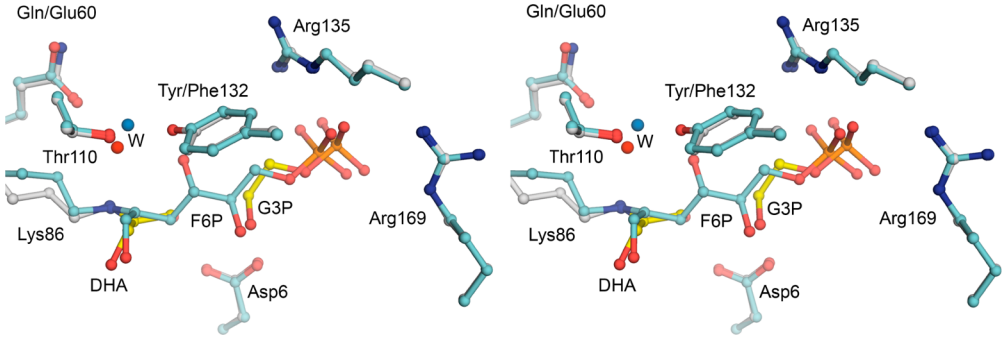

Figure 5. Superposition of the DHA Schiff base in *Tac*TAL Glu60Gln/Phe132Tyr (gray) with the F6P Schiff base in *Tac*TAL wt (light blue, PDB entry 3S1V) shown in stereoview. The DHA moiety and adjacent G3P are colored yellow. The catalytic water (W) is shown as a red sphere (DHA Schiff base) or a blue sphere (F6P Schiff base).

(3.74 Å) for a direct interaction, the spatial position of Tyr132 would allow a geometrically favorable (linear) and stereospecific proton transfer onto C3 with good frontier orbital overlap (Figure 4c). Alternatively, a synchronized proton transfer involving Tyr132 and the catalytic water may take place, although the geometry of proton transfer is less favorable (~30° deviation from linearity, no orbital overlap). Also, when judged on the basis of fitted *B* factors, the side chain of Tyr132 displays the highest flexibility of any active site residue (*B* factors are almost twice as high as those of neighboring side chains), supporting a mechanism in which Tyr132 could directly protonate C3. This structural flexibility could be key to a putative multifunctional role of Tyr132 in the studied "transaldolase-made-aldolase" Glu60Gln/Phe132Tyr variant, where proton transfers are required at different positions of the substrate in several steps of catalysis (2-OH, 4-OH, and C3) (see Scheme 1). Residue Asp6, the only other residue at the active site of the variant, which, from a chemical point of view, could potentially assist in proton transfers, is not suitably positioned to act as an acid–base catalyst. This lends further credence to a mechanism according to which Tyr132 is a multifunctional residue with critical roles in numerous proton transfers (either directly or via the adjacent water) along the catalytic cycle of *Tac*TAL Glu60Gln/Phe132Tyr.

A superposition of the DHA Schiff base trapped in *Tac*TAL Glu60Gln/Phe132Tyr with the previously characterized F6P Schiff base bound to *Tac*TAL wt highlights a conserved substrate binding mode in both enzymes, although they exhibit

DOI: 10.1021/acs.biochem.5b00283
Biochemistry 2015, 54, 4475–4486

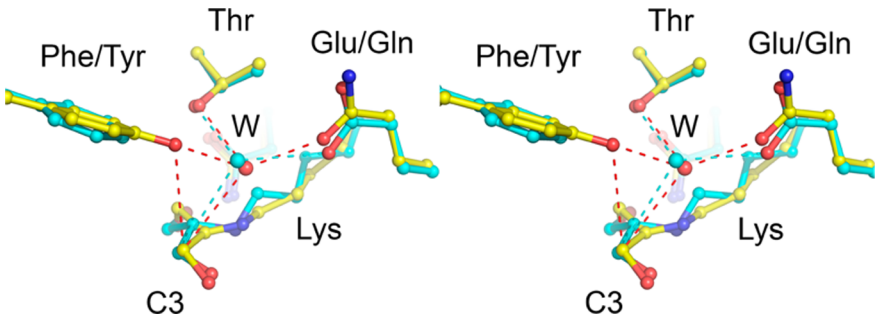

Figure 6. Superposition of the DHA Schiff base trapped in *Tac*TAL Glu60Gln/Phe132Tyr (yellow) with the borohydride-reduced DHA Schiff base in *E. coli* TAL (cyan, PDB entry 1UCW) shown in stereoview. H-Bonding interactions of <3.3 Å are indicated by dashed lines. The catalytic water (W) is shown as a red sphere (DHA Schiff base) or a cyan sphere (borohydride-reduced DHA Schiff base).

different reaction specificities (aldolase in the variant vs transaldolase in wt) (Figure 5). There are only very minor structural changes that can be detected for most active site side chains with roles in substrate binding and catalysis; even the mutated residues (Gln60 vs Glu60 and Tyr132 vs Phe132) occupy almost identical positions. The side chain of Lys86 adopts a slightly more extended conformation in the case of *Tac*TAL Glu60Gln/Phe132Tyr, whereas it is more U-shaped in the case of the wt enzyme. As expected, liberated product G3P in the variant is bound closer to the active site entrance (slightly distant from the C3 intermediate) than the corresponding moiety of the F6P Schiff base in wt *Tac*TAL as a result of bond cleavage and reactant separation. The phosphate moiety of G3P has moved by ~0.75 Å (chain B) or 0.9 Å (chain C) relative to that of the corresponding F6P Schiff base in these subunits in *Tac*TAL wt. Notably, the active site water in the variant is bound closer to the intermediate than the correponding catalytic water in *Tac*TAL wt with a bound F6P Schiff base (displacements of 1.0 Å in chain B and 0.6 Å in chain C). It resembles in this regard the binding position of the catalytic water in authentic FSA (see Figure 1). The more distant position of the catalytic water in *Tac*TAL wt could be key for preventing protonation of the carbanion-enamine intermediate formed upon cleavage of the F6P Schiff base. In *Tac*TAL wt with a bound F6P Schiff base, the catalytic water is suitably positioned for facilitating proton transfers between acid−base catalyst Glu60 and the ionizable C4-OH group of the intermediate as required for substrate cleavage (interatomic distance exemplified for chain B, 2.90 Å for O_{Glu60}−O_{water} and 2.61 Å for O_{water}−$O4_{Schiff\ base}$). However, the interatomic distance between the catalytic water and C3 would be too long (4.1 Å) and has unfavorable geometry for transfer of a proton from Glu60 onto C3 of the carbanion−enamine intermediate formed upon substrate cleavage. Unless substrate cleavage leads to a marked structural reorganization of the C3 lysyl conjugate, this could explain why TALs possess only very little aldolase activity. This hypothesis is further supported by structural comparison of *Tac*TAL Glu60Gln/Phe132Tyr in complex with the DHA Schiff base and the borohydride-reduced DHA Schiff base trapped in *E. coli* TAL wt (Figure 6).[29] In the latter structure, the catalytic water is bound more distant from C3 of the intermediate (3.7 Å) compared to the transaldolase-made-aldolase *Tac*TAL variant, and the potential transfer of a proton from Glu60 via the catalytic water onto C3 would have unfavorable geometry in the case of *E. coli* TAL, too.

Apart from direct interactions of the DHA Schiff base intermediate with active site residues and the immediate implications for the enzymatic mechanism, we could detect large-scale conformational dynamics that might be important for catalysis. As noted above, the two active sites of the homopentamer in the asymmetric unit that contain the Schiff base (chains B and C) are in the "closed" conformation, while the other subunits (A, D, and E) without the substrate or intermediate adopt the "open" state. A superposition of a "closed" and an "open" active site showcases (Figure 7) the fact

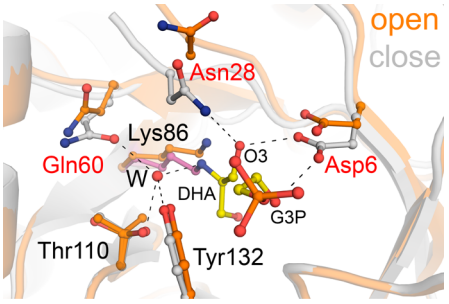

Figure 7. Superposition of a "closed" and "open" active site in *Tac*TAL Glu60Gln/Phe132. The "closed" active site of subunit B with the bound DHA Schiff base (gray) has been superposed with the "open" subunit E (ochre). Selected amino acid residues, the catalytic water (W), and H-bonding interactions of <3.3 Å are indicated. Note the different positions of residues Asp6, Asn28, and Gln60 (colored red) and the associated changes of the H-bonding interactions (see the text).

that numerous residues of the flexible N-terminal segment are engaged in binding of the substrate as, for example, Asp6 and Asn28 form H-bonds with the substrate. In addition, Gln60 (Glu in *Tac*TAL wt) seems to be repositioned in the course of substrate processing.

CONCLUSIONS

Our kinetic and structural studies of *Tac*TAL have provided novel insights into the reaction mechanisms of transaldolase and of the related F6P aldolase FSA. While a multifunctional glutamate (Glu60 in *Tac*TAL) is acting as a bona fide acid−base catalyst in numerous proton-transfer steps along the catalytic cycle of TAL (Scheme 1), a tyrosine is critically involved in the analogous reaction steps in authentic or engineered F6P aldolases (Tyr131 in FSA and Tyr132 in *Tac*TAL Glu60Gln/Phe132Tyr). A swapping of the acid−base catalysts, that is substitution of the TAL-specific Glu with Gln (as in FSA) and simultaneous introduction of the aldolase-specific Tyr in an engineered *Tac*TAL Glu60Gln/Phe132Tyr

DOI: 10.1021/acs.biochem.5b00283
Biochemistry 2015, 54, 4475−4486

double variant, conferred aldolase activity as the main activity to TAL with a catalytic efficiency that is even higher than that of authentic FSA or of single-site TAL variants, where both the catalytic Glu and Tyr are present (Table 1).[2,13] Steady-state and pre-steady-state kinetic analysis of *Tac*TAL wt and variants indicates that F6P binding and processing are greatly impaired when Glu and Tyr are both present as, for example, in the *Tac*TAL Phe132Tyr variant. In contrast, *Tac*TAL wt (Glu60 as the sole catalyst) and the engineered "pseudo-FSA" *Tac*TAL Glu60Gln/Phe132Tyr variant (Tyr132 as the sole catalyst) efficiently bind and cleave F6P with similar rate constants (k_{obs}) of 50 s^{-1}, implying that the initial steps of catalysis are not rate-determining and can be efficiently catalyzed by different residues at different positions. Cocrystallization of the "trans-aldolase-made-aldolase" *Tac*TAL Glu60Gln/Phe132Tyr double variant with substrate F6P allowed the structural characterization of the DHA Schiff base intermediate for the first time in this enzyme family. The structure suggests a key catalytic role of the introduced Tyr for aldolase-specific protonation of the carbanion−enamine intermediate (and similarly for the Tyr in FSA). A structural comparison between F6P aldolase and TALs lends credence to the hypothesis that the spatial position of the multifunctional residue (Glu in TAL and Tyr in FSA) is a critical determinant of reaction specificity. While a protonation of the common carbanion−enamine intermediate in TAL by the Glu-water dyad is geometrically not favorable, in terms of both distance and orbital overlap, the Tyr in FSA is suitably positioned for a direct and stereospecific protonation of the C3-centered lone pair formed upon cleavage of the F6P Schiff base. We suspect that both residues would be protonated in the carbanion−enamine state as they are likely deprotonating the substrate 4-OH in the preceding substrate cleavage step (see Scheme 1); therefore, in principle, both residues could deliver a proton to the carbanion−enamine intermediate. Apart from either favorable (FSA) or unfavorable (TAL) geometry for the transfer of a proton onto C3, subtle differences of the whole H-bonding network in TAL and FSA might further count as determinants of reaction specificity (Figure 8). While the protonated Glu in TAL would serve as a H-bond donor to the catalytic water, our structural data of the engineered TAL-derived aldolase pinpoint the fact that changing Glu to Gln also results in a switch in the polarity of the local hydrogen bond network as this residue is now acting as a H-bond acceptor. This might explain why the double variant (Glu to Gln and Phe to Tyr) displays 20-fold increased aldolase activity (increased k_{cat}, lowered K_M) compared to that of the Phe to Tyr single variant. To gain more definitive insights in this regard, a high-resolution structural characterization of the carbanion−enamine intermediate in TAL will be required. Our mechanistic proposition is corroborated by the assigned roles of catalytic residues in the related and mechanistically well understood FBP aldolase, where a multifunctional Glu (substrate binding and cleavage) and a Tyr located at the flexible C-terminus (protonation of the carbanion−enamine intermediate) act in tandem as acid−base catalysts.[9,30,31] Remarkably, both side chains are bound in similar positions relative to the catalytic Lys as the corresponding catalytic Glu and Tyr residues in TAL and FSA, respectively (Figure 8). The utilization of a Tyr for protonation of the carbanion−enamine intermediate in both FSA and FBP aldolase points to a unique feature of this side chain. It seems likely that a Tyr, purely based on pK_a considerations, is better suited to ensuring the reversibility of protonation of the carbanion−enamine intermediate.

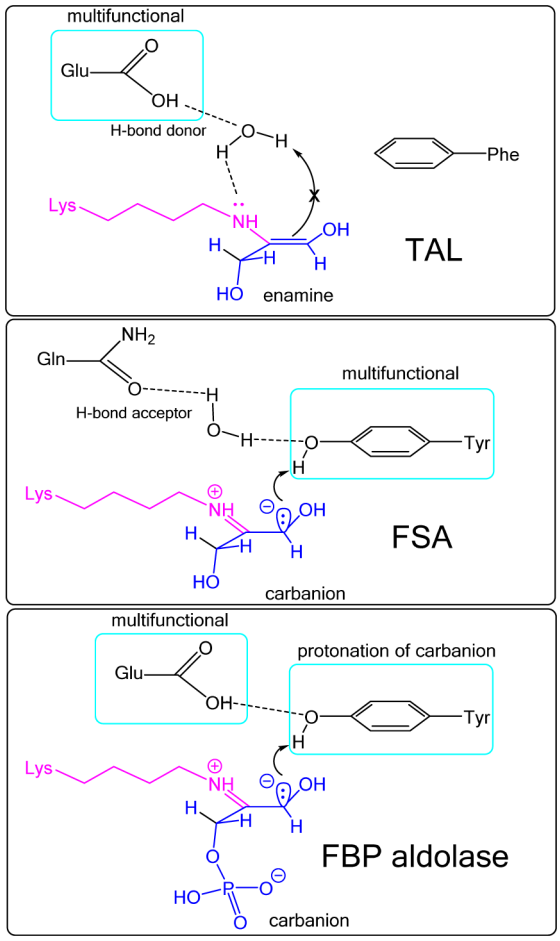

Figure 8. Catalytic functions and positions of key acid−base residues at the active sites of TAL, FSA, and FBP aldolase relative to the common carbanion−enamine intermediate and critical H-bonding interactions. In TAL, a multifunctional Glu catalyzes proton transfers via a catalytic water in the course of substrate binding, dehydration, and substrate cleavage but does not protonate C3 of the carbanion−enamine intermediate (likely stabilized as enamine). The Glu is thought to act as a H-bond donor. In FSA, a multifunctional Tyr catalyzes the analoguous reactions and additionally protonates the carbanion as it directly points to the C3 atom of the carbanion allowing for favorable geometry of proton transfer. Note the different H-bond network compared to that of TAL due to the fact that FBP aldolase is a "hybrid catalyst" of TAL and FSA and uses a multifunctional Glu for all acid−base steps until substrate cleavage, while a Tyr is critically involved in protonation of the carbanion. The active site position of this Tyr is almost identical to that found in FSA.

Large-scale structural rearrangements of *Tac*TAL that can be best described as a rigid-body movement of the N-terminus (residues 1−55) affording a more "open" or "closed" conformation are detectable.[5] The question of whether the observed structural changes are linked to catalysis remains to be answered.[32] The exclusive accumulation of the "closed" state for complexes with covalent reaction intermediates (F6P Schiff base, DHA Schiff base) indicates that a conformational lock-in (active site closure) is likely required for efficient substrate processing. One might speculate that formation of the "open" conformation and the associated alleviated interaction between enzyme and substrate (e.g., both Asp6 and Asn28 form H-bonds with substrate only in the "closed" conformation) would allow the products to more easily depart from the active site. In support of this notion is the exclusive observation of bound

DOI: 10.1021/acs.biochem.5b00283
Biochemistry 2015, 54, 4475−4486

G3P in the "closed" subunits (B and C in *Tac*TAL Glu60Gln/Phe132Tyr). In the case of the *Tac*TAL double variant, there is kinetic evidence that the opening and closing take place in the millisecond time regime. This process cannot be resolved by stopped-flow kinetics for the wt enzyme, suggesting a different time scale of active site closing and opening. Apart from the mechanistic implications for TAL and FSA catalysis as discussed above, the newly generated *Tac*TAL double Glu60Gln/Phe132Tyr variant with greatly stimulated aldolase activity seems to be a promising candidate for biocatalytic applications in the context of asymmetric C−C bond formation (reverse reaction of cleavage).[33]

AUTHOR INFORMATION

Corresponding Author

*E-mail: ktittma@gwdg.de. Phone: +49-551-3914430. Fax: +49-551-395749.

Notes

The authors declare no competing financial interest.

ACKNOWLEDGMENTS

We thank Piotr Neumann for data collection at beamline ID23-1 at ESRF, Grenoble, France, and discussion. We thank Ralf Ficner for access to the in-house rotating anode for crystal testing.

ABBREVIATIONS

TAL, transaldolase; *Tac*TAL, TAL from *T. acidophilum*; *Ec*TAL, TAL from *E. coli*; *Hs*TAL, TAL from *Homo sapiens*; FSA, fructose-6-phosphate aldolase; F6P, D-fructose 6-phosphate; G3P, D-glyceraldehyde 3-phosphate; E4P, D-erythrose 4-phosphate; S7P, D-sedoheptulose 7-phosphate; DHA, dihydroxyacetone; PDB, Protein Data Bank.

REFERENCES

(1) Horecker, B. L., Pontremoli, S., Ricci, C., and Cheng, T. (1961) On the nature of the transaldolase-dihydroxyacetone complex. *Proc. Natl. Acad. Sci. U. S. A. 47*, 1949−1955.

(2) Schurmann, M., and Sprenger, G. A. (2001) Fructose-6-phosphate aldolase is a novel class I aldolase from Escherichia coli and is related to a novel group of bacterial transaldolases. *J. Biol. Chem. 276*, 11055−11061.

(3) Tittmann, K. (2014) Sweet siblings with different faces: the mechanisms of FBP and F6P aldolase, transaldolase, transketolase and phosphoketolase revisited in light of recent structural data. *Bioorg. Chem. 57*, 263−280.

(4) Thorell, S., Schurmann, M., Sprenger, G. A., and Schneider, G. (2002) Crystal structure of decameric fructose-6-phosphate aldolase from Escherichia coli reveals inter-subunit helix swapping as a structural basis for assembly differences in the transaldolase family. *J. Mol. Biol. 319*, 161−171.

(5) Lehwess-Litzmann, A., Neumann, P., Parthier, C., Ludtke, S., Golbik, R., Ficner, R., and Tittmann, K. (2011) Twisted Schiff base intermediates and substrate locale revise transaldolase mechanism. *Nat. Chem. Biol. 7*, 678−684.

(6) Light, S. H., Minasov, G., Duban, M. E., and Anderson, W. F. (2014) Adherence to Burgi-Dunitz stereochemical principles requires significant structural rearrangements in Schiff-base formation: insights from transaldolase complexes. *Acta Crystallogr., Sect. D: Biol. Crystallogr. 70*, 544−552.

(7) Sygusch, J., Beaudry, D., and Allaire, M. (1987) Molecular architecture of rabbit skeletal muscle aldolase at 2.7-A resolution. *Proc. Natl. Acad. Sci. U. S. A. 84*, 7846−7850.

(8) Berthiaume, L., Tolan, D. R., and Sygusch, J. (1993) Differential Usage of the Carboxyl-Terminal Region among Aldolase Isozymes. *J. Biol. Chem. 268*, 10826−10835.

(9) St-Jean, M., and Sygusch, J. (2007) Stereospecific proton transfer by a mobile catalyst in mammalian fructose-1,6-bisphosphate aldolase. *J. Biol. Chem. 282*, 31028−31037.

(10) Rose, I. A., O'Connell, E. L., and Mehler, A. H. (1965) Mechanism of the Aldolase Reaction. *J. Biol. Chem. 240*, 1758−1765.

(11) Lorentzen, E., Pohl, E., Zwart, P., Stark, A., Russell, R. B., Knura, T., Hensel, R., and Siebers, B. (2003) Crystal structure of an archaeal class I aldolase and the evolution of (betaalpha)8 barrel proteins. *J. Biol. Chem. 278*, 47253−47260.

(12) Lorentzen, E., Siebers, B., Hensel, R., and Pohl, E. (2005) Mechanism of the Schiff base forming fructose-1,6-bisphosphate aldolase: structural analysis of reaction intermediates. *Biochemistry 44*, 4222−4229.

(13) Schneider, S., Sandalova, T., Schneider, G., Sprenger, G. A., and Samland, A. K. (2008) Replacement of a phenylalanine by a tyrosine in the active site confers fructose-6-phosphate aldolase activity to the transaldolase of Escherichia coli and human origin. *J. Biol. Chem. 283*, 30064−30072.

(14) Lehwess-Litzmann, A., Neumann, P., Golbik, R., Parthier, C., and Tittmann, K. (2011) Crystallization and preliminary X-ray diffraction analysis of transaldolase from Thermoplasma acidophilum. *Acta Crystallogr., Sect. F: Struct. Biol. Cryst. Commun. 67*, 584−586.

(15) Kabsch, W. (2010) Xds. *Acta Crystallogr., Sect. D: Biol. Crystallogr. 66*, 125−132.

(16) Emsley, P., and Cowtan, K. (2004) Coot: model-building tools for molecular graphics. *Acta Crystallogr., Sect. D: Biol. Crystallogr. 60*, 2126−2132.

(17) Adams, P. D., Afonine, P. V., Bunkoczi, G., Chen, V. B., Davis, I. W., Echols, N., Headd, J. J., Hung, L. W., Kapral, G. J., Grosse-Kunstleve, R. W., McCoy, A. J., Moriarty, N. W., Oeffner, R., Read, R. J., Richardson, D. C., Richardson, J. S., Terwilliger, T. C., and Zwart, P. H. (2010) PHENIX: a comprehensive Python-based system for macromolecular structure solution. *Acta Crystallogr., Sect. D: Biol. Crystallogr. 66*, 213−221.

(18) Winn, M. D., Ballard, C. C., Cowtan, K. D., Dodson, E. J., Emsley, P., Evans, P. R., Keegan, R. M., Krissinel, E. B., Leslie, A. G., McCoy, A., McNicholas, S. J., Murshudov, G. N., Pannu, N. S., Potterton, E. A., Powell, H. R., Read, R. J., Vagin, A., and Wilson, K. S. (2011) Overview of the CCP4 suite and current developments. *Acta Crystallogr., Sect. D: Biol. Crystallogr. 67*, 235−242.

(19) Chen, V. B., Arendall, W. B., 3rd, Headd, J. J., Keedy, D. A., Immormino, R. M., Kapral, G. J., Murray, L. W., Richardson, J. S., and Richardson, D. C. (2010) MolProbity: all-atom structure validation for macromolecular crystallography. *Acta Crystallogr., Sect. D: Biol. Crystallogr. 66*, 12−21.

(20) Holm, L., and Rosenstrom, P. (2010) Dali server: conservation mapping in 3D. *Nucleic Acids Res. 38*, W545−549.

(21) Di Tommaso, P., Moretti, S., Xenarios, I., Orobitg, M., Montanyola, A., Chang, J. M., Taly, J. F., and Notredame, C. (2011) T-Coffee: a web server for the multiple sequence alignment of protein and RNA sequences using structural information and homology extension. *Nucleic Acids Res. 39*, W13−17.

(22) Tsolas, O., and Joris, L. (1975) Transaldolase. *Methods Enzymol. 42*, 290−297.

(23) Hartley, B. S., and Kilby, B. A. (1952) The Inhibition of Chymotrypsin by Diethyl Para-Nitrophenyl Phosphate. *Biochem. J. 50*, 672−678.

(24) Hartley, B. S., and Kilby, B. A. (1954) The Reaction of Para-Nitrophenyl Esters with Chymotrypsin and Insulin. *Biochem. J. 56*, 288−297.

(25) Hammes, G. G., Chang, Y. C., and Oas, T. G. (2009) Conformational selection or induced fit: a flux description of reaction mechanism. *Proc. Natl. Acad. Sci. U. S. A. 106*, 13737−13741.

(26) Abel, M., Planas, A., and Christensen, U. (2001) Presteady-state kinetics of Bacillus 1,3−1,4-beta-glucanase: binding and hydrolysis of a 4-methylumbelliferyl trisaccharide substrate. *Biochem. J. 357*, 195−202.

DOI: 10.1021/acs.biochem.5b00283
Biochemistry 2015, 54, 4475−4486

(27) Vogt, A. D., and Di Cera, E. (2012) Conformational selection or induced fit? A critical appraisal of the kinetic mechanism. *Biochemistry 51*, 5894−5902.
(28) Vogt, A. D., Pozzi, N., Chen, Z., and Di Cera, E. (2014) Essential role of conformational selection in ligand binding. *Biophys. Chem. 186*, 13−21.
(29) Jia, J., Schorken, U., Lindqvist, Y., Sprenger, G. A., and Schneider, G. (1997) Crystal structure of the reduced Schiff-base intermediate complex of transaldolase B from Escherichia coli: mechanistic implications for class I aldolases. *Protein Sci. 6*, 119−124.
(30) Maurady, A., Zdanov, A., de Moissac, D., Beaudry, D., and Sygusch, J. (2002) A conserved glutamate residue exhibits multifunctional catalytic roles in D-fructose-1,6-bisphosphate aldolases. *J. Biol. Chem. 277*, 9474−9483.
(31) St-Jean, M., Lafrance-Vanasse, J., Liotard, B., and Sygusch, J. (2005) High resolution reaction intermediates of rabbit muscle fructose-1,6-bisphosphate aldolase: substrate cleavage and induced fit. *J. Biol. Chem. 280*, 27262−27270.
(32) Bhabha, G., Lee, J., Ekiert, D. C., Gam, J., Wilson, I. A., Dyson, H. J., Benkovic, S. J., and Wright, P. E. (2011) A dynamic knockout reveals that conformational fluctuations influence the chemical step of enzyme catalysis. *Science 332*, 234−238.
(33) Szekrenyi, A., Soler, A., Garrabou, X., Guerard-Helaine, C., Parella, T., Joglar, J., Lemaire, M., Bujons, J., and Clapes, P. (2014) Engineering the donor selectivity of D-fructose-6-phosphate aldolase for biocatalytic asymmetric cross-aldol additions of glycolaldehyde. *Chem. - Eur. J. 20*, 12572−12583.

DOI: 10.1021/acs.biochem.5b00283
Biochemistry 2015, 54, 4475−4486